Journal of Stress Analysis
Vol. 6, No. 1, Spring – Summer 2021, 13-28
Bu-Ali Sina University

ORIGINAL RESEARCH PAPER

An Analytical Solution to the Problem of Thin-walled Pressure Vessel with Circular-arc Cross-section

M. Salmani-Tehrani*, **Z. Dehghanian**
Department of Mechanical Engineering, Isfahan University of Technology, Isfahan, Iran.

Article info

Article history:
Received 22 April 2021
Received in revised form
06 July 2021
Accepted 27 July 2021

Keywords:
Thin-walled pressure vessel
Surface of revolution
Circular-arc generating curve
Stress distribution
Analytical solution

Abstract

Design procedure of pressure vessels is very important due to their vast applications in many industries. This procedure is mainly based on determining the stress and strain distribution, which is resulted from the internal pressure. In this paper a thin-walled pressure vessel of circular-arc cross-section is analytically studied. The vessel is a surface of revolution generated by rotating a circular arc about an axis that neither intersects the arc nor necessarily passes through the arc center. Both convex and concave vessels with open- and closed-end conditions are considered. The equilibrium equations for a proper element of the vessel surface are derived and solved analytically. Assuming small deformation and elastic behavior for the vessel, the integral constant is determined based on the end boundary conditions of the vessel. Since this type of pressure vessel was not studied in the previous literature, the results of present model are compared with similar ABAQUS Finite Element (FE) simulation. A very close agreement was observed. This evidently implies the validity of the presented model.

Nomenclature

C	Integration constant	p	Internal pressure
t	Vessel thickness	R	The radius of the generative circular arc
d	The distance between the arc center and the axis of symmetry	$\hat{\mathbf{n}}_\varphi, \hat{\mathbf{n}}_\theta, \hat{\mathbf{n}}_R$	Unit vectors in φ^-, θ^- and R-direction, respectively
r	The distance between an arbitrary point P on the vessel surface to the symmetry axis	r_α	The distance between the vessel edge the axis of symmetry
φ	Angular position of an arbitrary point P on the vessel surface	z	Dimensionless distance between the arc center and the axis of symmetry
t_α	Vessel thickness along the $\varphi = \alpha$ edge	$\sigma_\theta, \sigma_\varphi$	Hoop and longitudinal components of stress, respectively
α	The angle of Half of the angel of the vessel		

1. Introduction

Pressure vessels have a wide range of industrial applications. Among different types of vessels, thin-walled vessels (with radius-to-thickness ratio of 10 or greater) of cylindrical and spherical shapes are more popular. Closed-end, as well as open-end cylindrical thin-walled pressure vessels are extensively used to store liquids

*Corresponding author: M. Salmani-Tehrani (Assistant Professor)
E-mail address: tehrani@iut.ac.ir
http://dx.doi.org/10.22084/jrstan.2021.24014.1179
ISSN: 2588-2597

and fluids. The stress state in a pressure vessel involves only the three normal stress components in longitudinal, radial, and hoop directions. Of course for thin-walled vessels the radial stress component is neglected compared with the two other components [1].

Most of the previous works focused on stress analysis in cylindrical and spherical vessels. Only a few studies on the vessels other than cylindrical and spherical shapes have been reported. Bargman [2] attempted to predict the failure in pressure vessels. Assuming presence of some initial defects, such as crack, the effect of initial defects on the failure of the vessel was studied. Hwang and Lin [3] utilized finite element simulation to study free bulging in tube hydroforming. Based on assuming an ellipsoidal surface for the tube during forming process, a mathematical model was developed. Strano and Altan [4] proposed an inverse energy approach to determine stress distribution across the tube wall in the tube hydroforming. In this research, the tube profile was approximated by a cosine-like function and then according to volume constancy, the wall thickness was calculated. They showed that if the stress-strain curve which is obtained by this method is used as the input to Finite Element (FE) simulation, the results would show a better accuracy. Rahimi and Roozegar [5] analyzed the elastic-plastic behavior of a cylindrical vessel with different types of lids, such as spherical, elliptical, and coil shapes. They also considered a nozzle on the lid and analyzed the effect of type and thickness of the lid and existence of nozzle on limit plastic load and yield stress. Abrinia and Dehghani [6] investigated the elastic-plastic behavior of a thick-walled cylindrical vessel under sudden internal pressure. The effect of work-hardening coefficient, strain rate, and temperature were taken into consideration in their models. Boumaiza et al. [7] studied plastic instability of a tube in bulging test. They showed that for short tubes the effect of geometric changes should be taken into account. Lopes et al. [8] studied the effect of initial geometric imperfections on the plastic stability of a thick-walled cylinder under internal pressure, using both numerical and experimental approaches. Djavanroodi et al. [9] analyzed free bulge tube hydroforming process analytically and numerically. In their analytical approach, it was assumed that the cylindrical tube remains cylindrical during forming.

Velasco and Boudeau [10] presented a theoretical analysis for tube bulging test. In this study, the bulged zone was assumed to be axially symmetric. An area enclosed by two circular arcs with different radii was considered for the tube wall in bulge zone. The analytical results, including the pole thickness during the test, final thickness over the whole bulged zone, and the stress-strain curve were validated by comparing with FE simulation results. Bortot et al. [11] dealt with studying the stress state in tube hydroforming process. In this research, an analytical model coupled with experiments to obtain stress-strain curve. Comparing the analytical results by Finite Element (FE) simulation, it was shown that a good agreement exists. Ben Ouirane et al. [12] tried to evaluate the error on experimental stress-strain curve obtained from tube bulging test. For this purpose the experimental results were compared with those of the analytical model proposed in Ref. [10]. Boudeau and Male´cot [13] presented a simplified analytical model for tube bulging test. Based on Finite Element (FE) simulations, the profile of the tube in the bulging test was approximated by a circular arc. The stress distribution was then calculated based on the analytical model of Ref. [10]. Kru˙zelecki and Proszwoski [14] dealt with optimization of the shape of the lid for a thin-walled pressure vessel. Two different types of single- and double-arc profiles were considered in this regard. Using numerical optimization, a single-arc profile of polynomial type was proposed for the lid. Chaaba [15] studied the plastic collapse of a thin-walled pressure vessel, considering large deformation and strain hardening effects. He et al. [16] developed an analytical model for free tube bulging. In this model, the equilibrium for an element at the central point in the bulge zone (the section with the maximum bulge height) was examined. Assuming that axial stress component for this element should be the same as in cylindrical shell, the stress components for this element were determined. The profile of the bulged tube was fitted by an elliptical curve. To validate the analysis, the model prediction was compared with similar Finite Element (FE) simulation results and a good correlation was reported. In another work, He et al. [17] proposed a linear variation of thickness of the tube wall in bulging process. This assumption was then incorporated into the analytical model presented in their previous work [16], to derive the equivalent stress-strain relation for the central point in the bulge zone (the section with the maximum bulge height). The analytically computed stress-strain curve was collated with that of obtained from the simple tension test and an acceptable agreement was observed. Zamaninejad and Fatehi [18] dealt with the elastic-plastic deformation of a rotating thick-walled cylindrical pressure vessel, under uniform internal and external pressure. The state of deformation was assumed to be plane-strain. Tresca's yield criterion along with elastic-ideal plastic stress-strain relation was used to model the material behavior. The model also accounted for the density variation. Babeshko et al. [19] utilized numerical simulation to investigate the stress-strain state and the strength of a thin-walled pressure vessel under high pressure. Ibrahim et al. [20] discussed the stress distribution in thin-walled cylindrical and spherical pressure vessels. Applying the static equilibrium equations for a special part of the vessel, the stress components were consequently calculated. As a case study, the strain components on the wall of a soda can be ex-

perimentally measured. Assuming elastic deformation, the experimental strains and Hook's law were used in the stresses obtained from the model, to evaluate the internal pressure of the can. Mulder et al. [21] used optical measuring system in the bulge test to determine the flow curves. They saw that if the coordinates of the cross-section of the tube was estimated by an ellipsoid shape, the maximum accuracy was achieved. Also using two equilibrium equations for stresses of the tube and assuming a linear variation of the thickness strain, they could approximate the stresses of the tube wall. Cui et al. [22] analyzed the bulging process of thick-walled aluminum alloy tubes under double-sided pressure experimentally and numerically. In this research, the stress distribution was obtained by finite element simulation and the effect of external pressure on bulging parameter, such as bulging profile and tube thickness was studied. Liu et al. [23] presented an analytical model to determine the pressure-time loading profile for free tube bulging. In this study, the tube line in the free bulging zone was recognized as an ellipse. Furthermore, the axial stress was considered as this in cylindrical tube and the circumferential stress can be derived from equilibrium equation. Cui et al. [24] characterized the stress-strain response of double-sided pressure tube bulging test. For stress calculation, they used analytical model that was expressed in Ref. [16]. Wu et al. [25] using three-dimensional digital image correlation method and fitting a curve through the coordinate data, extracted the tube profile during bulging. Then by using equilibrium equation for an element in the middle of the tube, stresses were obtained. Finally finite element simulation was used for the validation of the method. Song and Hui [26] calculated the forming pressure of corrugated tubes using incremental plasticity theory. The profile of tube during bulging was an arc and the equilibrium equation for an element at the middle of the arc was extracted. Then by considering longitudinal stress as in cylindrical tube, hoop stress was obtained. Numerical simulation and experiments were also done for validation of explained model.

As previously pointed out, the majority of the published studies dealt with studying deformation analysis of cylindrical and spherical vessels. To the best knowledge of authors, the pressure vessel with circular-arc cross-section was not considered. Of course in some of the studies in free tube bulge test, such as Ref. [10,12,13], the profile of the bulged tube was assumed to be a circular arc. However, in these studies, in some parts of the equilibrium equations, the curvature of the generative arc has been ignored but in this study the curvature of the arc is considered in all equations. In the present paper, a thin-walled pressure vessel with circular-arc cross-section is analytically studied and closed-form equations for stress distribution are derived. The vessel surface is generated by rotating a circular arc about an axis that neither intersect the arc nor necessarily pass through the arc center. Both convex and concave vessels with open- and closed-end conditions are considered. The analytical equations obtained in this paper can be used to determine stress distribution in similar geometries, such as bulged zone in free tube bulging process and toroidal surfaces like vehicle's tires. Then for an element of the vessel surface, equilibrium equations are extracted and by solving these equations analytically stress distribution on the vessel surface is determined. In order to verify the results, the obtained results were compared with finite element simulation by ABAQUS software. Finally, by introducing the non-dimensional stresses, effect of geometrical parameters of cross section on distribution of non-dimensional stresses are studied.

2. Differential Equations of Equilibrium and Analytical Solution

In this paper a vessel with circular-arc cross-section under internal pressure is analytically studied. As shown in Fig. 1, the vessel is a surface of revolution which is generated by rotating a circular arc (generative arc) about an axis of symmetry. The symmetry axis neither intersects the arc nor necessarily passes through the arc center. Both of convex and concave vessels are shown in this figure. As it can be seen from the figure, in convex vessel the symmetry axis and the arc center are both located on the same side of the arc. On the other hand in concave vessel the arc lies between the symmetry axis and the arc center. In the following of this section, the governing differential equations for the both convex and concave vessel are derived. Due to uncommon geometry of the vessel surface, a proper surface element is used for this purpose. Then the equilibrium equations are analytically solved to determine the stress distribution within the vessel.

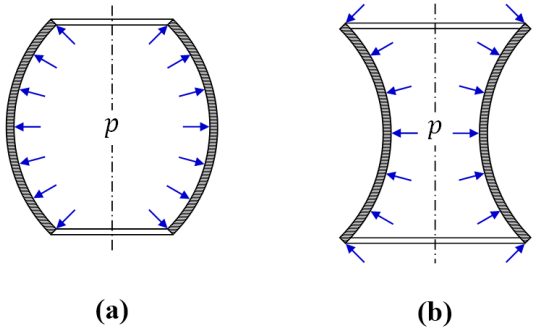

Fig. 1. Schematic representation of a thin-walled pressure vessel with circular-arc cross-section; a) Convex vessel, b) Concave vessel.

2.1. Convex Vessel

Fig. 2 shows the geometry of the generative arc for a convex vessel. In this figure z-axis is the symme-

try axis and point O' is the center of the generative arc. Because of the symmetry of the vessel with respect to xy-planes, only one half of the arc is shown. The distance between an arbitrary point P on the vessel surface, to the symmetry axis, is denoted by r. The radial distance r is a function of the angle φ and is given by Eq. (1).

$$r = R\cos\varphi - d \tag{1}$$

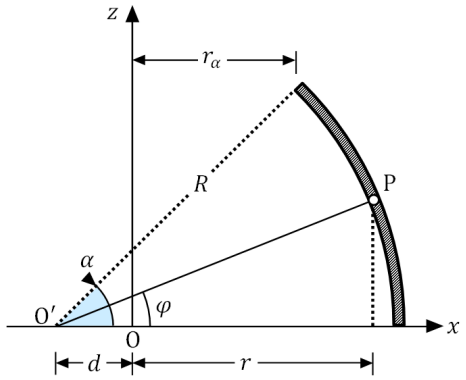

Fig. 2. Section geometry for a convex vessel with circular-arc cross-section.

In Eq. (1), R is the arc radius and d denotes for the distance between the arc center and the symmetry axis (Fig. 2). It is worth reminding that R, d, and α in Eq. (1) are constant parameters of the section which don't depend on the variable φ.

To derive the differential equations of equilibrium, the equilibrium of a surface element of the vessel is examined. The surface element ABCD illustrated in Fig. 3, is generated by rotating the arc element MN about the z-axis, through a small angle $d\theta$. In this figure, the arc element MN (with the length of $Rd\varphi$), and hence its center O', lies in xz-plane. This means that the xz-plane is the plane of symmetry for this element. Moreover, the colored zone $A'B'C'D'$ in the figure represents the projection of the surface element ABCD on the xy-plane.

In order to express the equilibrium equations in component form, five outward unit vectors are introduced based on the element geometry. These include four unit vectors perpendicular to the midpoint of the four edge sides of the element (AB, BC, CD, AD) and one unit vector perpendicular to the midpoint of element face. These unit vectors can be easily shown in 2D views as illustrated in Fig. 3. It should be noted that the unit vectors perpendicular to the edges AB and CD ($\hat{\mathbf{n}}_\theta^{\text{Left}}$ and $\hat{\mathbf{n}}_\theta^{\text{Right}}$ respectively) are parallel to the xy-plane.

According to Fig. 3b, the unit vectors perpendicular to the top and bottom sides of ABCD surface element, in the Cartesian coordinates, are given by Eqs. (2) and (3).

$$\hat{\mathbf{n}}_\varphi^{\text{Bot}} = +\sin(\varphi^{\text{Bot}})\hat{\mathbf{i}} - \cos(\varphi^{\text{Bot}})\hat{\mathbf{k}} \tag{2}$$

$$\hat{\mathbf{n}}_\varphi^{\text{Top}} = -\sin(\varphi^{\text{Top}})\hat{\mathbf{i}} + \cos(\varphi^{\text{Top}})\hat{\mathbf{k}} \tag{3}$$

The angles φ^{Bot} and φ^{Top} are obtained from Eqs. (4) and (5) (Fig. 3b).

$$\varphi^{\text{Bot}} = \varphi - \frac{1}{2}d\varphi \tag{4}$$

$$\varphi^{\text{Top}} = \varphi + \frac{1}{2}d\varphi \tag{5}$$

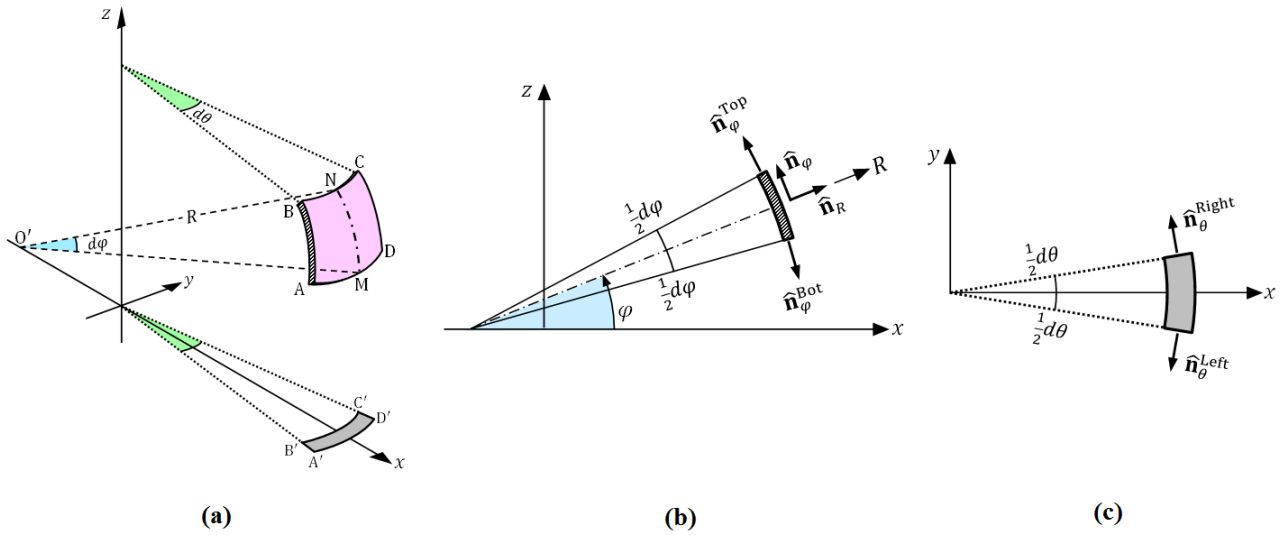

Fig. 3. Representation of an arbitrary element for a covex vessel, a) 3D representation, b) 2D view in xz-plane, c) 2D view in xy-plane.

Substituting Eqs. (4) and (5) into (2) and (3) and given that $d\varphi$ is a very small angle, Eqs. (2) and (3) are rewritten as (6) and (7).

$$\hat{\mathbf{n}}_{\varphi}^{\mathrm{Bot}} = \left(\sin\varphi - \frac{1}{2}\cos\varphi d\varphi\right)\hat{\mathbf{i}} - \left(\cos\varphi + \frac{1}{2}\sin\varphi d\varphi\right)\hat{\mathbf{k}} \tag{6}$$

$$\hat{\mathbf{n}}_{\varphi}^{\mathrm{Top}} = -\left(\sin\varphi + \frac{1}{2}\cos\varphi d\varphi\right)\hat{\mathbf{i}} + \left(\cos\varphi - \frac{1}{2}\sin\varphi d\varphi\right)\hat{\mathbf{k}} \tag{7}$$

Similarly, unit vectors perpendicular to the right and left sides of ABCD surface element, in the Cartesian coordinates, are expressed by Eqs. (8) and (9).

$$\hat{\mathbf{n}}_{\theta}^{\mathrm{Left}} = -\frac{1}{2}d\theta\hat{\mathbf{i}} - \hat{\mathbf{j}} \tag{8}$$

$$\hat{\mathbf{n}}_{\theta}^{\mathrm{Right}} = -\frac{1}{2}d\theta\hat{\mathbf{i}} + \hat{\mathbf{j}} \tag{9}$$

According to the Fig. 3b, unit vectors in R and φ directions are given by (10) and (11).

$$\hat{\mathbf{n}}_{R} = \cos\varphi\hat{\mathbf{i}} + \sin\varphi\hat{\mathbf{k}} \tag{10}$$

$$\hat{\mathbf{n}}_{\varphi} = -\sin\varphi\hat{\mathbf{i}} + \cos\varphi\hat{\mathbf{k}} \tag{11}$$

It should be noted that the unit vector $\hat{\mathbf{n}}_{\varphi}$ corresponds to the central point of element ABCD and$\hat{\mathbf{n}}_{\varphi}^{\mathrm{Bot}}$ and $\hat{\mathbf{n}}_{\varphi}^{\mathrm{Top}}$ vectors correspond to the bottom and top edges of the element, respectively.

Before proceeding to derive the equilibrium equations, the forces which are applied on the element ABCD should be introduced. Stresses on the surface element ABCD consist of the internal pressure applied on the internal surface, $\hat{\sigma}_{\varphi}^{\mathrm{Top}}$ and $\hat{\sigma}_{\varphi}^{\mathrm{Bot}}$ which act on the top and bottom sides and $\sigma_{\theta}^{\mathrm{Left}}$ and $\sigma_{\theta}^{\mathrm{Right}}$ acting on the left and right sides of the surface element. Assuming isotropic behavior for the vessel and uniform thickness in θ direction, the problem is an axially-symmetric one. This implies that all field variables are independent of θ, and hence $\sigma_{\theta}^{\mathrm{Right}} = \sigma_{\theta}^{\mathrm{Left}} = \sigma_{\theta}$. Moreover the equilibrium along the hoop direction is automatically satisfied due to the axial symmetry. Therefore only two independent equilibrium equations exist for the element. The equilibrium in R direction, with corresponding unit vector $\hat{\mathbf{n}}_{R}$ (shown in Fig. 3), is first examined.

$$\sum F_R = 0 \quad \therefore$$

$$p(Rd\varphi r d\theta) + \sigma_{\varphi}^{\mathrm{Top}}(t^{\mathrm{Top}}r^{\mathrm{Top}}d\theta)(\hat{\mathbf{n}}_{\varphi}^{\mathrm{Top}}\cdot\hat{\mathbf{n}}_{R}) + \sigma_{\varphi}^{\mathrm{Bot}}(t^{\mathrm{Bot}}r^{\mathrm{Bot}}d\theta)(\hat{\mathbf{n}}_{\varphi}^{\mathrm{Bot}}\cdot\hat{\mathbf{n}}_{R}) + \sigma_{\theta}(tRd\varphi)(\hat{\mathbf{n}}_{\theta}^{\mathrm{Left}}\cdot\hat{\mathbf{n}}_{R} + \hat{\mathbf{n}}_{\theta}^{\mathrm{Right}}\cdot\hat{\mathbf{n}}_{R}) = 0 \tag{12}$$

In Eq. (12) t^{Top} and r^{Top} denote for thickness of the top edge and distance between top edge to the symmetry axis, respectively. Similarly, t^{Bot} and r^{Bot} are defined for the bottom edge AD, t and r indicate the thickness and distance from the symmetry axis at the central point of the surface element. The dot product of unit vectors in Eq. (12) is appeared to determine the projection of each force along R-direction. Substituting unit vectors from Eqs. (3), (4), (9), (10) and (11) and dividing by $(d\theta d\varphi)$, the result is simplified as Eq. (13).

$$\sigma_{\varphi}rt + Rt\sigma_{\theta}\cos\varphi = Rrp \tag{13}$$

In Eq. (13), the term $(\sigma_{\varphi}tr)$, which has been replaced for $\frac{1}{2}(\sigma_{\varphi}^{\mathrm{Top}}t^{\mathrm{Top}}r^{\mathrm{Top}} + \sigma_{\varphi}^{Bot}t^{\mathrm{Bot}}r^{\mathrm{Bot}})$ in Eq. (12), refers to the value of the expression evaluated at the central point of the surface element. Eq. (13) is rearranged as (14).

$$\frac{\sigma_{\varphi}}{R} + \frac{\sigma_{\theta}}{r}\cos\varphi = \frac{p}{t} \tag{14}$$

Now equilibrium in φ-direction, with corresponding unit vector $\hat{\mathbf{n}}_{\varphi}$, is examined.

$$\sum F_{\varphi} = 0 \quad \therefore$$

$$\sigma_{\varphi}^{\mathrm{Top}}(t^{\mathrm{Top}}r^{\mathrm{Top}}d\theta)(\hat{\mathbf{n}}_{\varphi}^{\mathrm{Top}}\cdot\hat{\mathbf{n}}_{\varphi}) + \sigma_{\varphi}^{\mathrm{Bot}}(t^{\mathrm{Bot}}r^{\mathrm{Bot}}d\theta)(\hat{\mathbf{n}}_{\varphi}^{\mathrm{Bot}}\cdot\hat{\mathbf{n}}_{\varphi}) + \sigma_{\theta}(tRd\varphi)(\hat{\mathbf{n}}_{\theta}^{\mathrm{Left}}\cdot\hat{\mathbf{n}}_{\varphi} + \hat{\mathbf{n}}_{\varphi}^{\mathrm{Right}}\cdot\hat{\mathbf{n}}_{\varphi}) = 0 \tag{15}$$

Again by substituting the unit vectors from Eqs. (2), (3), (8), (9), and (11) in (15) and dividing by $d\theta$, Eq. (16) is obtained.

$$(\sigma_{\varphi}^{\mathrm{Top}}t^{\mathrm{Top}}r^{\mathrm{Top}} - \sigma_{\varphi}^{\mathrm{Bot}}t^{\mathrm{Bot}}r^{\mathrm{Bot}}) + (\sigma_{\theta}Rt)d\varphi\sin\varphi = 0 \tag{16}$$

The term $(\sigma_{\varphi}^{\mathrm{Top}}t^{\mathrm{Top}}r^{\mathrm{Top}} - \sigma_{\varphi}^{\mathrm{Bot}}t^{\mathrm{Bot}}r^{\mathrm{Bot}})$ in Eq. (16) means a very small variation of $(\sigma_{\varphi}tr)$, from the bottom edge AD to the top edge BC. Replacing this term by $d(\sigma_{\varphi}tr)$, Eq. (16) can be rewritten as (17).

$$d(\sigma_{\varphi}tr) + (\sigma_{\theta}Rt)\sin\varphi d\varphi = 0 \tag{17}$$

Substitutingσ_θ in terms of σ_φ from Eq. (14), Eq. (17) can be written in the form of Eq. (18).

$$d(\sigma_\varphi tr) + Rrt\tan\varphi\left(\frac{p}{t} - \frac{\sigma_\varphi}{R}\right)d\varphi = 0 \qquad (18)$$

Multiplying both sides of Eq. (18) by $\cos\varphi$ and dividing by $d\varphi$, Eq. (19) is obtained.

$$\frac{d(\sigma_\varphi rt)}{d\varphi}\cos\varphi - (\sigma_\varphi rt)\sin\varphi = -(Rrp)\sin\varphi \qquad (19)$$

Eq. (19) can be rewritten as the differential Eq. (20).

$$\frac{d(\sigma_\varphi rt\cos\varphi)}{d\varphi} = -(Rrp)\sin\varphi \qquad (20)$$

On the right hand side of Eq. (20), (Rp) is constant, while the term $(r\sin\varphi)$ is a function of φ. Substituting r from Eq. (1) and integrating with respect to φ, Eq. (21) is obtained.

$$\sigma_\varphi = \frac{R^2p}{rt}\left(\frac{1}{2}\cos\varphi - \frac{d}{R} + \frac{C}{\cos\varphi}\right) \qquad (21)$$

In Eq. (21), C is the constant of integration. Now, substituting for σ_φ from Eq. (21) into Eq. (14), results in Eq. (22) for σ_θ.

$$\sigma_\theta = \frac{Rp}{t}\left(\frac{1}{2} - \frac{C}{(\cos\varphi)^2}\right) \qquad (22)$$

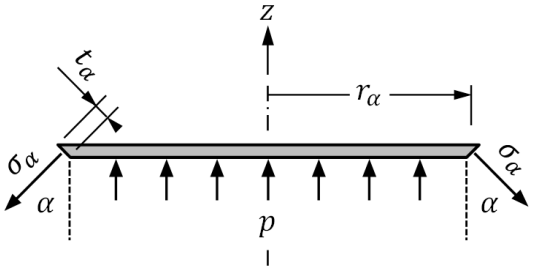

Fig. 4. Illustrating the forces acting on the lid of a convex vessel.

The integral constant C is determined based on σ_φ-boundary condition, on the vessel edge ($\varphi = \alpha$). For an open-end vessel, the free stress boundary condition is applied, as Eq. (23).

$$\sigma_\alpha = \sigma_\varphi(\varphi = \alpha) = 0 \qquad (23)$$

Consequently, the constant C is obtained as Eq. (24).

$$C = (\cos\alpha)^2\left(-\frac{1}{2} + \frac{d}{R\cos\alpha}\right) \qquad (24)$$

Now substituting C into Eqs. (21) and (22), σ_φ and σ_θ are given by Eqs. (25) and (26).

$$\left(\frac{t}{R}\right)\left(\frac{\sigma_\varphi}{p}\right) = \frac{1}{\left(\frac{\cos\varphi}{\cos\alpha}\right) - \left(\frac{d}{R\cos\alpha}\right)} \times \left[\frac{1}{2}\left(\frac{\cos\varphi}{\cos\alpha} - \frac{\cos\alpha}{\cos\varphi}\right) - \left(\frac{d}{R\cos\alpha}\right)\left(1 - \frac{\cos\alpha}{\cos\varphi}\right)\right] \qquad (25)$$

$$\left(\frac{t}{R}\right)\left(\frac{\sigma_\theta}{p}\right) = \frac{1}{2} + \frac{1}{2}\left(\frac{\cos\alpha}{\cos\varphi}\right)^2 - \left(\frac{d}{R\cos\alpha}\right)\left(\frac{\cos\alpha}{\cos\varphi}\right)^2 \qquad (26)$$

For closed-end vessel, the σ_φ which is applied on the vessel edge (at $\varphi = \alpha$) should be determined through the static equilibrium of the lid. As illustrated in Fig. 4, it is assumed that on the top edge, along which the lid is connected to the vessel, only σ_φ is. Thus, using the equilibrium equation for the lid in z-direction, the stress σ_φ along the $\varphi = \alpha$ edge is obtained as equation (27).

$$\sigma_\alpha = \sigma_\varphi(\varphi = \alpha) = \frac{p(\pi r_\alpha^2)}{(2\pi r_\alpha t_\alpha)\cos\alpha} \qquad (27)$$

In Eq. (27), t_α is the vessel thickness along $\varphi = \alpha$ edge. Radial distance r_α and the angle α are also shown in Fig. 4. According to this figure, r_α is determined from Eq. (28).

$$r_\alpha = R\cos\alpha - d \qquad (28)$$

Consequently, using boundary condition (27) and substituting r_α from (28), the integral constant C in (21) is obtained as Eq. (29).

$$C = \frac{1}{2}\left(\frac{d}{R}\right)^2 \qquad (29)$$

Finally, by substituting C from (29) into (21) and (22), stress components for a convex closed-end vessel are given by Eqs. (30) and (31).

$$\left(\frac{t}{R}\right)\left(\frac{\sigma_\varphi}{p}\right) = \frac{1}{\left(\frac{\cos\varphi}{\cos\alpha}\right) - \left(\frac{d}{R\cos\alpha}\right)} \times \left[\frac{1}{2}\left(\frac{\cos\varphi}{\cos\alpha}\right) - \left(\frac{d}{R\cos\alpha}\right) - \frac{1}{2}\left(\frac{d}{R\cos\alpha}\right)^2\left(\frac{\cos\alpha}{\cos\varphi}\right)\right] \qquad (30)$$

$$\left(\frac{t}{R}\right)\left(\frac{\sigma_\theta}{p}\right) = \frac{1}{2} - \frac{1}{2}\left(\frac{d}{R\cos\alpha}\right)^2\left(\frac{\cos\alpha}{\cos\varphi}\right)^2 \qquad (31)$$

2.2. Concave Vessel

Similar to convex vessel, Fig. 5 shows one-half of the arc cross-section of the concave vessel with z-axis as the

symmetry axis and point O' as the arc center. According to this figure, the distance between an arbitrary P point on the section to the symmetry axis, which is denoted by r, is determined in terms of the corresponding angel φ from Eq. (32).

$$r = d - R\cos\varphi \tag{32}$$

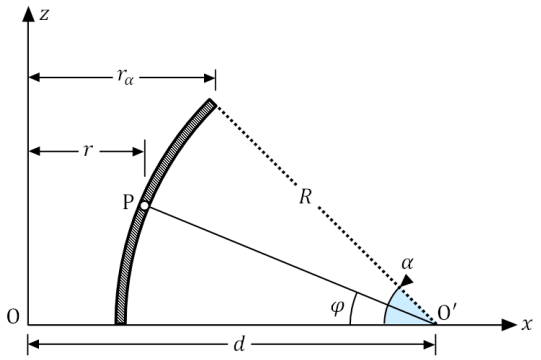

Fig. 5. Representation of the cross-section of the concave vessel.

Similar to Eq. (1), in Eq. (32) R is the arc radius and d is the distance between arc center (point O') to symmetry axis (z-axis) (Fig. 5). Moreover, R, d and α, are constant parameters which don't depend on φ. Due to the similarity of equations with those of convex vessel, only the final equations are presented for concave vessel. Equilibrium for an element of the concave vessel in R-direction leads to Eq. (33).

$$-\frac{\sigma_\varphi}{R} + \frac{\sigma_\theta}{r}\cos\varphi = \frac{p}{t} \tag{33}$$

Also Equilibrium in φ-direction is results in Eq. (34).

$$\frac{d(\sigma_\varphi r t\cos\varphi)}{d\varphi} = -(Rrp)\sin\varphi \tag{34}$$

Integrating (34) with respect to φ, Eq. (35) is obtained for σ_φ.

$$\sigma_\varphi = \frac{R^2 p}{rt}\left(\frac{1}{2}\cos\varphi - \frac{d}{R} + \frac{C}{\cos\varphi}\right) \tag{35}$$

Substituting σ_φ from (35) into (33), σ_θ is determined as Eq. (36).

$$\sigma_\theta = \frac{Rp}{t}\left(-\frac{1}{2} + \frac{C}{(\cos\varphi)^2}\right) \tag{36}$$

Similar to convex vessel, the integral constant C in (35) and (36) should be determined based on the end boundary condition of σ_φ in the vessel edge ($\varphi = \alpha$). For open-end condition, boundary condition the same as (23). Therefore Eq. (37) is obtained for the constant C.

$$C = (\cos\alpha)^2\left(-\frac{1}{2} + \frac{d}{R\cos\alpha}\right) \tag{37}$$

Substituting C from (37) into (35) and (36), stress components in φ- and θ-directions are obtained from Eqs. (38) and (39).

$$\left(\frac{t}{R}\right)\left(\frac{\sigma_\varphi}{p}\right) = \frac{1}{\left(\frac{d}{R\cos\alpha}\right) - \left(\frac{\cos\varphi}{\cos\alpha}\right)} \times \left[\frac{1}{2}\left(\frac{\cos\varphi}{\cos\alpha} - \frac{\cos\alpha}{\cos\varphi}\right) - \left(\frac{d}{R\cos\alpha}\right)\left(1 - \frac{\cos\alpha}{\cos\varphi}\right)\right] \tag{38}$$

$$\left(\frac{t}{R}\right)\left(\frac{\sigma_\theta}{p}\right) = -\frac{1}{2} - \frac{1}{2}\left(\frac{\cos\alpha}{\cos\varphi}\right)^2 + \left(\frac{d}{R\cos\alpha}\right)\left(\frac{\cos\alpha}{\cos\varphi}\right)^2 \tag{39}$$

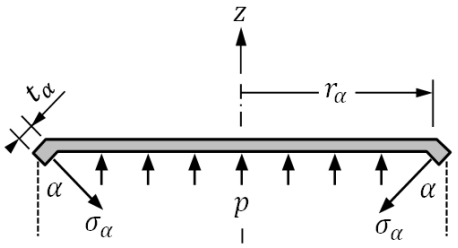

Fig. 6. Illustrating the forces acting on the lid of the concave vessel.

Similar to the convex vessel, for a closed-end concave vessel the integral constant C is determined from equilibrium of the lid in z-direction. Fig. 6 shows the lid for a concave vessel and the forces acting on it. Determining the constant C and substituting into (35) and (36) yield Eqs. (40) and (41) for stress component in a closed-end concave vessel.

$$\left(\frac{t}{R}\right)\left(\frac{\sigma_\varphi}{p}\right) = \frac{1}{\left(\frac{\cos\varphi}{\cos\alpha}\right) - \left(\frac{d}{R\cos\alpha}\right)} \times \left[\frac{1}{2}\left(\frac{\cos\varphi}{\cos\alpha}\right) - \left(\frac{d}{R\cos\varphi}\right) - \frac{1}{2}\left(\frac{d}{R\cos\alpha}\right)^2\left(\frac{\cos\alpha}{\cos\varphi}\right)\right] \tag{40}$$

$$\left(\frac{t}{R}\right)\left(\frac{\sigma_\theta}{p}\right) = -\frac{1}{2} + \frac{1}{2}\left(\frac{d}{R\cos\alpha}\right)^2\left(\frac{\cos\alpha}{\cos\varphi}\right)^2 \tag{41}$$

3. Finite Element Simulation

Because the vessel which was considered in the present work has not been studied before, the results of the presented model are compared with Finite Element (FE) simulations to verify the model. FE simulations were carried out using ABAQUS commercial software. As the problem is axisymmetric with one additional plane of symmetry, only one-half of the cross-section arc was modeled. Steel mechanical properties were assumed for the material behavior of the vessel (Table 1).

Table 1
Mechanical properties of the vessel in FE simulations [27].

E (GPa)	ν
200	0.3

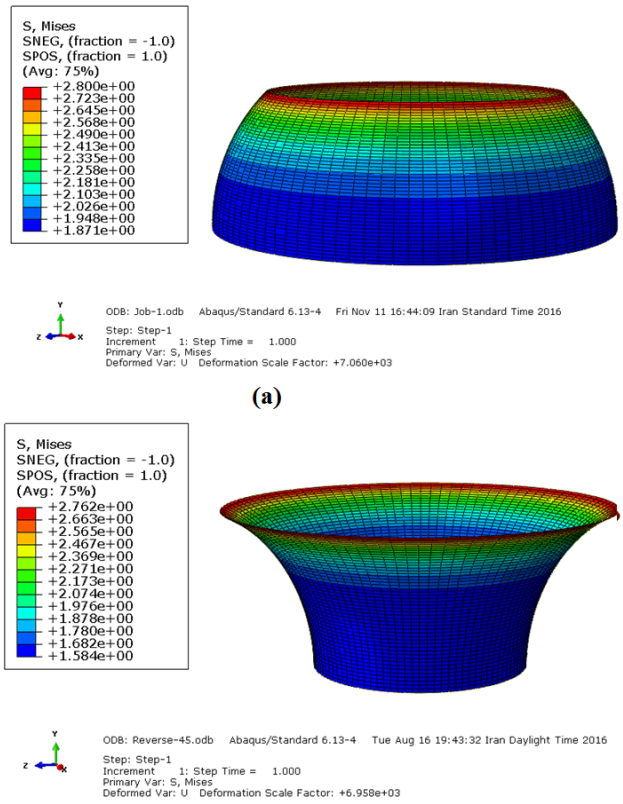

Fig. 7. FE model of the vessel, a) Convex vessel, and b) Concave vessel.

For an open-end vessel, free boundary condition was used for the vessel edge. On the other hand, for a closed-end vessel, in order to avoid stress concentration on the connection edge, an extra edge tangent to the arc was designed. Here, in order to define the joint between the vessel and the lid, the translational degrees of freedom of the edges of the vessel and lid were considered to be identical. A low internal pressure was applied to ensure small deformation. The vessel (with a radius of 0.2m) was meshed using 100 axisymmetric shell elements and the lid was modeled as an analytical rigid body. A single general static step was used for the analysis. After completing the simulation, longitudinal and hoop stress were extracted from simulations and compared with those of analytical model.

4. Results and Discussion

In this section the results of analytical model is first verified by comparing with Finite Element (FE) simulation. Then, the effect of geometrical parameters of cross-section on dimensionless stress components in longitudinal and hoop directions is investigated.

4.1. Model verification

Figs. 8 to 11 illustrate the comparison between dimensionless stresses obtained from analytical approach with similar results of FE simulations. In Figs. 8 and 9, the comparison is made between open-and closed-end convex vessels, respectively. Similarly Figs. 10 and 11 represent the results for open- and closed-end concave vessels. For more comprehensive investigation, in each of these figures the stress curve has been plotted for two different arc angles of $\alpha = 30°$ and $\alpha = 45°$. It is worth mentioning that for $\alpha = 45°$ in convex vessel, the arc center lies on the axis of symmetry. Therefore the stress state in within the vessel corresponds to the stress in a spherical thin-walled vessel under internal pressure. Consequently, the dimensionless stress components of σ_θ and σ_φ are equal to 0.5.

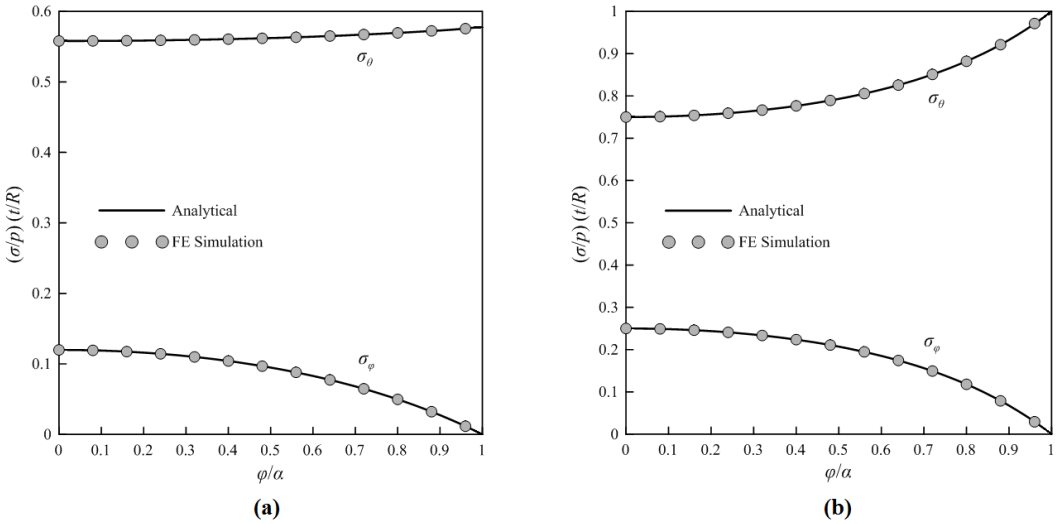

Fig. 8. Comparing between analytical and FE simulation results for dimensionless stress components, for an open-end convex vessel, a) $\alpha = 30°$, and b) $\alpha = 45°$.

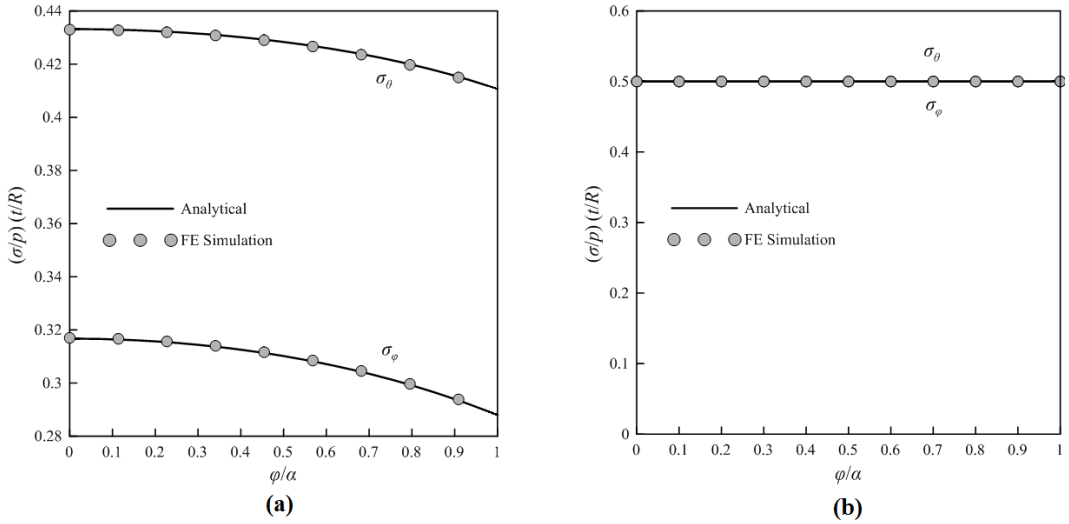

Fig. 9. Comparing between analytical and FE simulation results for dimensionless stress components, for an closed-end convex vessel, a) $\alpha = 30°$, and b) $\alpha = 45°$.

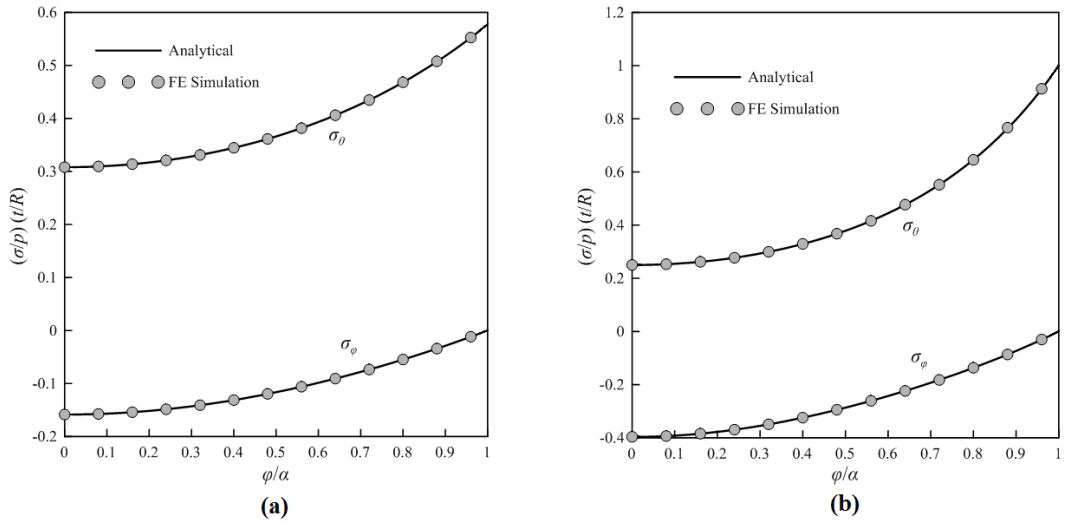

Fig. 10. Comparing between analytical and FE simulation results for dimensionless stress components, for an open-end concave vessel, a) $\alpha = 30°$, and b) $\alpha = 45°$.

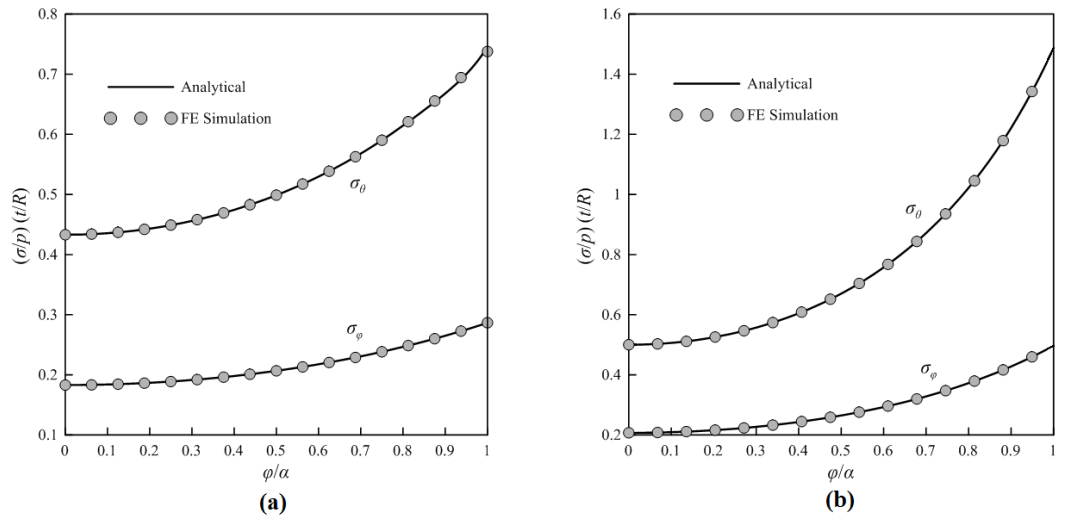

Fig. 11. Comparing between analytical and FE simulation results for dimensionless stress components, for an closed-end concave vessel, a) $\alpha = 30°$, and b) $\alpha = 45°$.

A very close agreement between analytical and FE simulation results is observed in Figs. 8 to 11. This evidently indicates the validity of the proposed analytical model. It should be mentioned that, since in the equilibrium equations of analytical solution, the curvature of the generative arc has not been ignored and the error between analytical solution and Finite Element (FE) simulation is negligible for vessels with different curvatures and for different input parameters.

4.2. Investigating the Effect of the Vessel Geometry

After the model was validated, a parametric study is now carried out to investigate the effect of geometric parameters. In this regard, the effect of the parameters by which the geometry of the vessel is defined, on the stress distribution, is analytically studied. To this end, according to the analytical equations for stress components, the dimensionless parameter z is defined as equation (42).

$$z = \frac{d}{R\cos\alpha} \tag{42}$$

In fact, the dimensionless parameter z indicates the dimensionless distance between the arc center and the symmetry axis. According to Fig. 5, the ranges of variation of z for convex and concave vessels are as inequalities (43).

$$z \leq 1 \quad , \qquad \text{Convex Vessel} \tag{43}$$

$$z \geq \frac{1}{\cos\alpha} \quad , \qquad \text{Concave Vessel} \tag{44}$$

As can be seen from Fig. 2, for convex vessel, a positive value of z implies that the arc and center of the arc are in opposite sides of the symmetry axis. However, a negative value of z means that both of the arc and its center are located at the same side of the symmetry axis. On the other hand, for concave vessel, both of the arc and its center are always located in the same side of the symmetry axis.

The geometric parameters which are to be investigated include the type of the vessel (convex or concave), the effect of the vessel end-conditions (with or without the lid), dimensionless distance z, and the angle of the arc, α. In Fig. 12 to 23 dimensionless stress components are plotted for open-end/closed-end convex/concave vessels, for three different values of α. In order to investigate the effect of the dimensionless distance z, in each case the curves corresponding to different values of z are reported. In these figures the horizontal axis indicates the normalized angle (φ/α), which specifies the longitudinal position of the point along the arc. As (φ/α) increases from 0 to 1, the point moves from the midpoint towards edge-point of the vessel (Fig. 2).

Figs. 12-14 and 15-17 are devoted to open-end and closed-end convex vessel, respectively. Similarly, Figs. 18-20 and 21-23 present the results for open-end and closed-end concave vessel, respectively.

According to the figures, for an open-end vessel (convex or concave), as expected, a zero longitudinal stress is observed on the vessel edge. There is, however, a difference between convex and concave vessel. The longitudinal stress in open-end convex vessel is positive, while for an open-end concave vessel the longitudinal stress is negative. This is due to the fact that in open-end convex vessel the internal pressure results in increasing the curvature of the section arc, which this, in turn, causes longitudinal tension in the vessel wall. But for a concave vessel the internal pressure make the vessel wall to be longitudinally compressed. Therefore it is expected that for open-end vessel, as the angle α increases, so does the longitudinal stress. On other hand for concave vessel, a reverse effect is expected. This is confirmed by the results shown in Figs. 12-14 and 18-20.

Another point about the results for open-end vessel is that, regardless of the stress sign, the hoop stress is much greater than the longitudinal. Furthermore, as the angle α decreases, not only does the magnitude of the longitudinal stress decrease, but also a more uniform distribution of longitudinal stress is observed. The reason is that as the angle α decreases, the vessel shape becomes more similar to a cylindrical vessel.

Note that for a closed-end convex vessel with $z = 0$, the stress state within the vessel wall become the same as a spherical vessel. This is an expected result because the arc center lies on the symmetry axis for $z = 0$. For this reason the stress curves for $z = 0$ in Figs. 15-17 are observed as a constant function (straight line) with the value equal to 0.5.

Concerning the effect of dimensionless distance z, the results reveal that, in general, as the arc gets far away from the symmetry axis, the longitudinal stress grows up for all the cases. Of course it should be remembered that based on the definition of the parameters d, hence z, for the arc to get far away from the symmetry axis, z should decrease below the zero and become more and more negative. However for concave vessel, the distance between the arc and the symmetry axis increases when z increases. A similar result holds for hoop stress, except for closed-end convex vessel. The reason of this stress growing is that as the arc gets farther away from the axis, the distance between the points on the section and the axis increases. A similar situation arises for a cylindrical pressure vessel when the radius of the cylinder increases. Of course, this is not the case for closed-end convex vessel. As can be seen from Eq. (31), the hoop stress in closed-end convex vessel depend on the square of z and, consequently, the sign of z does not affect on the hoop stress.

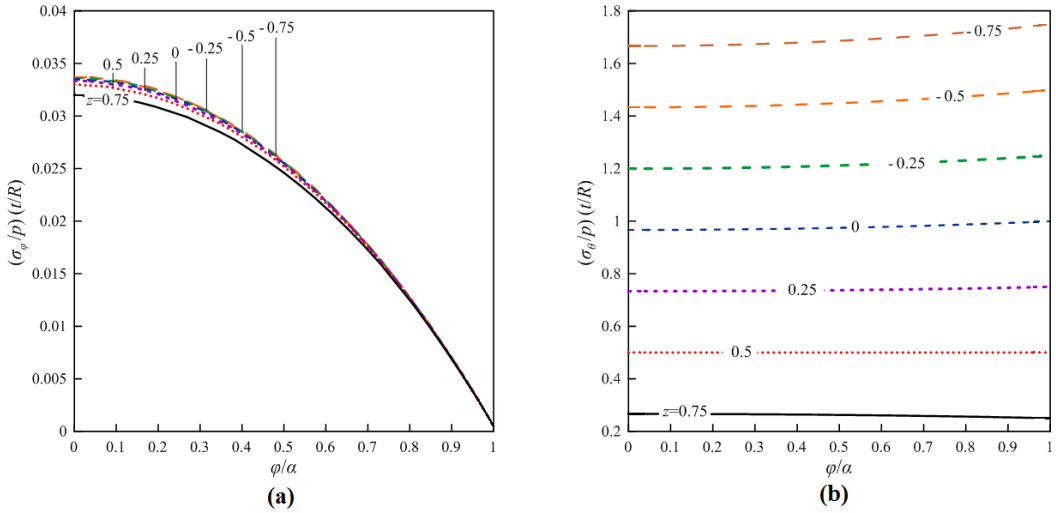

Fig. 12. Stress distribution for open-end convex vessel with $\alpha = 15°$, a) Longitudinal stress (σ_φ), and b) Hoop stress (σ_θ).

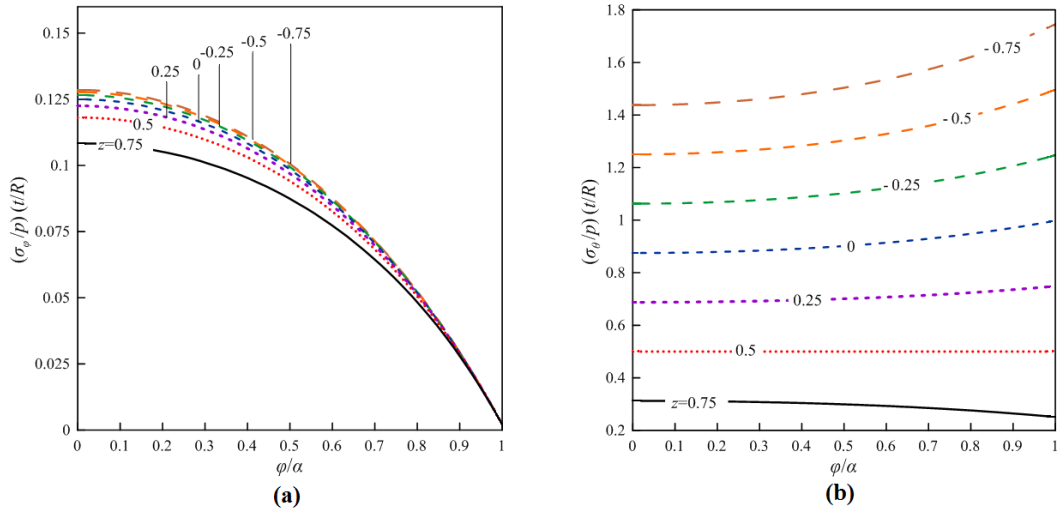

Fig. 13. Stress distribution for open-end convex vessel with $\alpha = 30°$, a) Longitudinal stress (σ_φ), and b) Hoop stress (σ_θ).

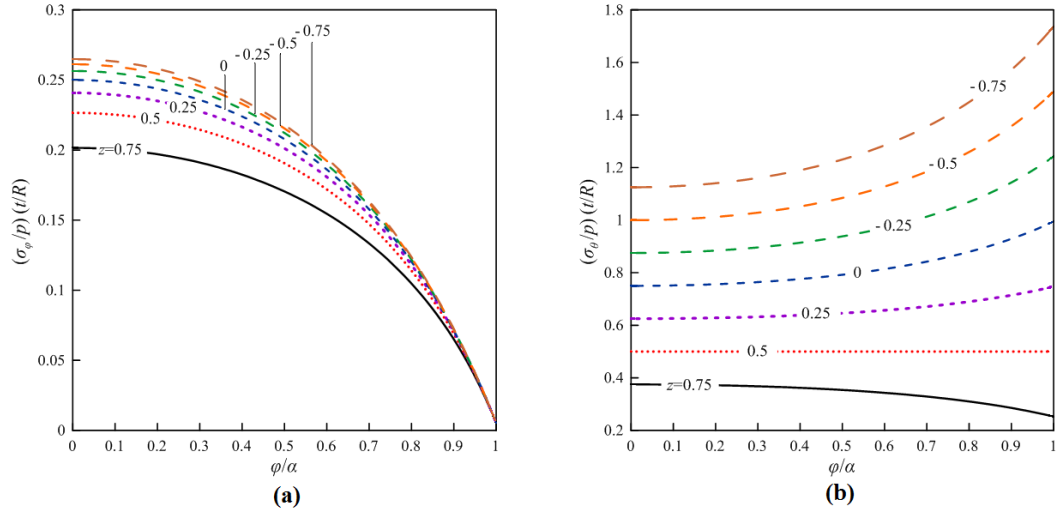

Fig. 14. Stress distribution for open-end convex vessel with $\alpha = 45°$, a) Longitudinal stress (σ_φ), and b) Hoop stress (σ_θ).

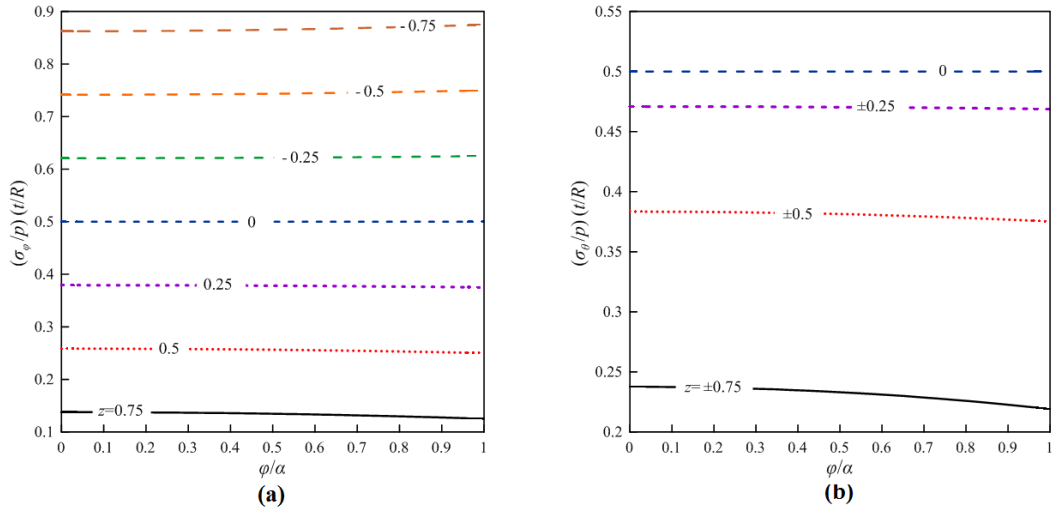

Fig. 15. Stress distribution for closed-end convex vessel with $\alpha = 15°$, a) Longitudinal stress (σ_φ), and b) Hoop stress (σ_θ).

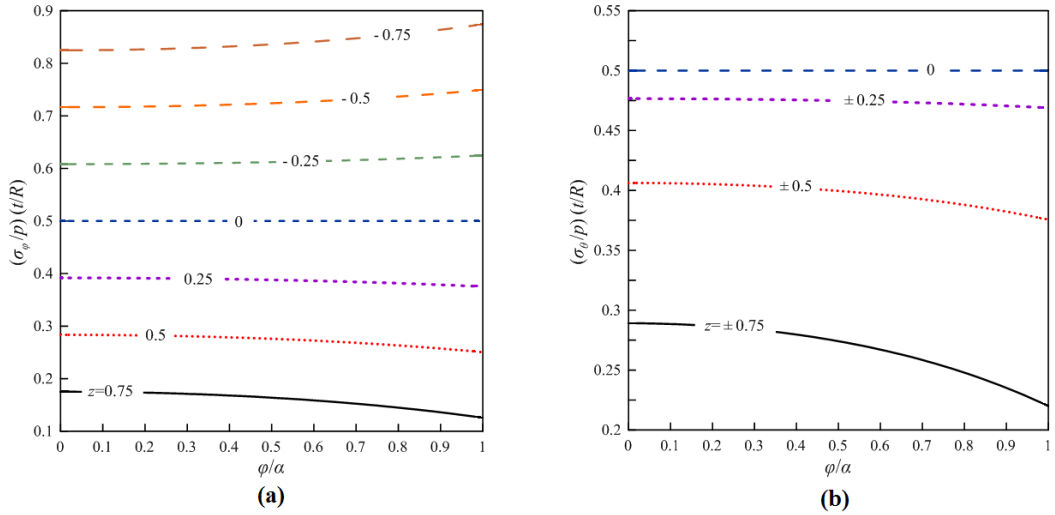

Fig. 16. Stress distribution for closed-end convex vessel with $\alpha = 30°$, a) Longitudinal stress (σ_φ), and b) Hoop stress (σ_θ).

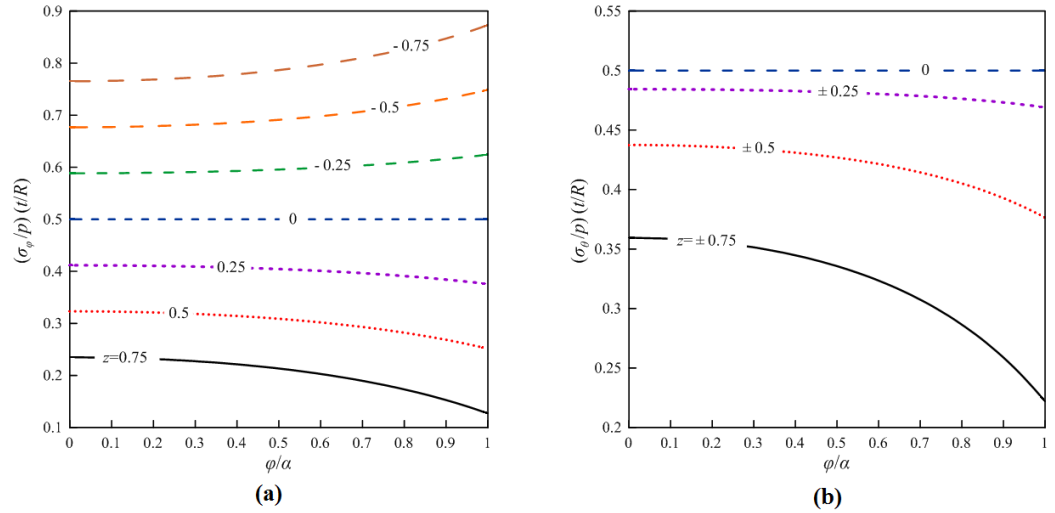

Fig. 17. Stress distribution for closed-end convex vessel with $\alpha = 45°$, a) Longitudinal stress (σ_φ), and b) Hoop stress (σ_θ).

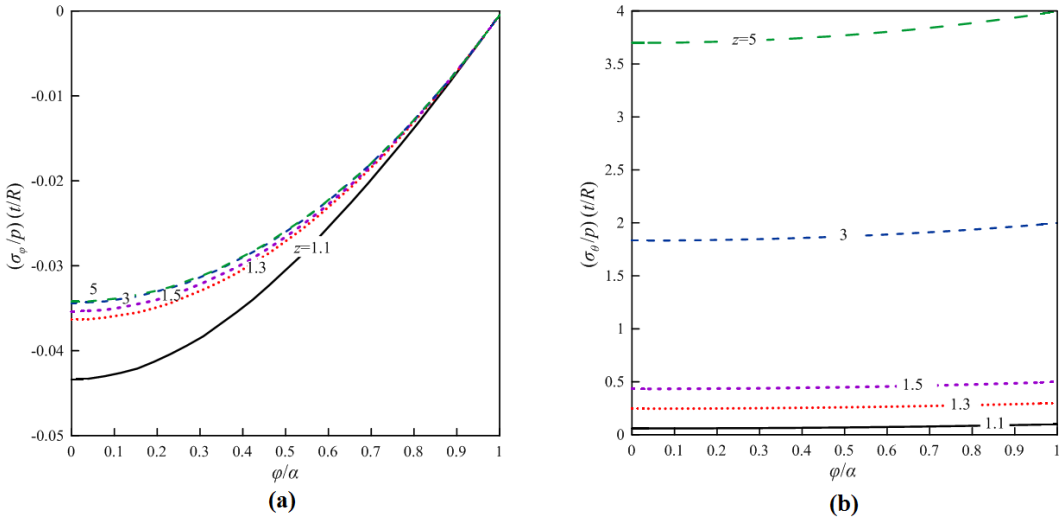

Fig. 18. Stress distribution for open-end concave vessel with $\alpha = 15°$, a) Longitudinal stress (σ_φ), and b) Hoop stress (σ_θ).

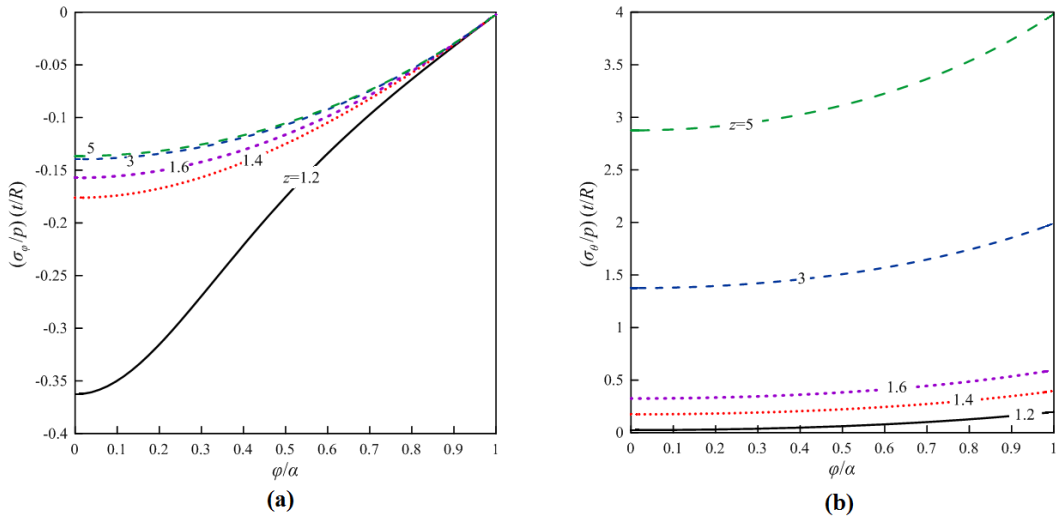

Fig. 19. Stress distribution for open-end concave vessel with $\alpha = 30°$, a) Longitudinal stress (σ_φ), and b) Hoop stress (σ_θ).

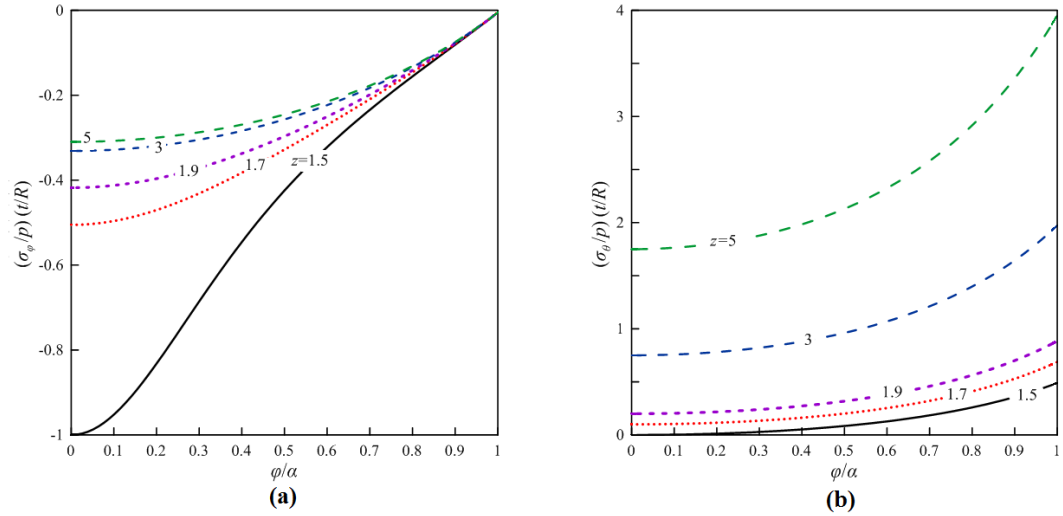

Fig. 20. Stress distribution for open-end concave vessel with $\alpha = 45°$, a) Longitudinal stress (σ_φ), and b) Hoop stress (σ_θ).

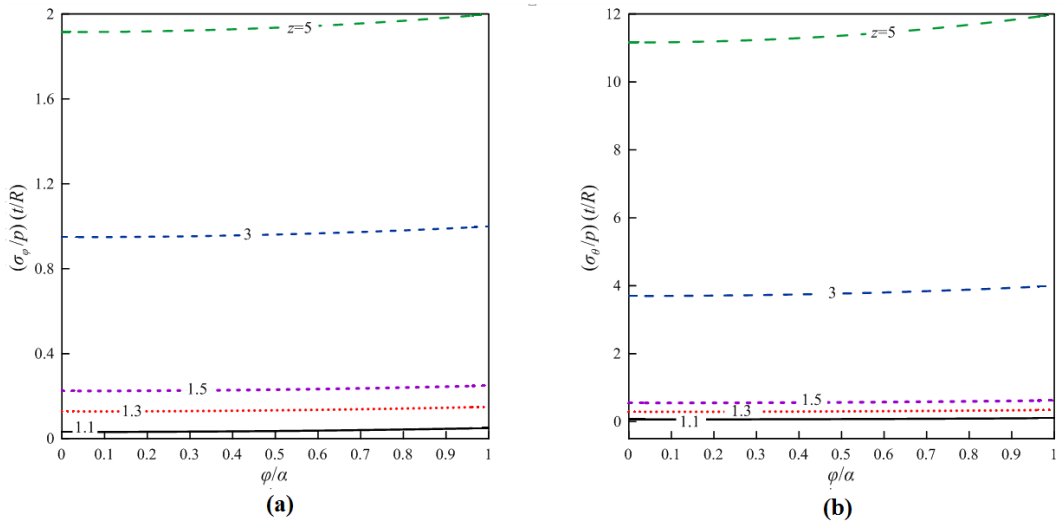

Fig. 21. Stress distribution for closed-end concave vessel with $\alpha = 15°$, a) Longitudinal stress (σ_φ), and b) Hoop stress (σ_θ).

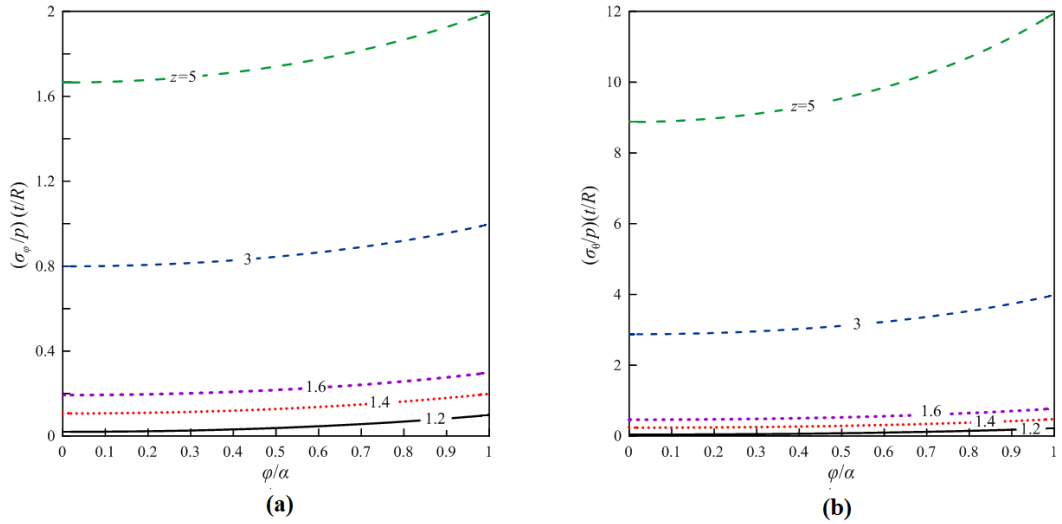

Fig. 22. Stress distribution for closed-end concave vessel with $\alpha = 30°$, a) Longitudinal stress (σ_φ), and b) Hoop stress (σ_θ).

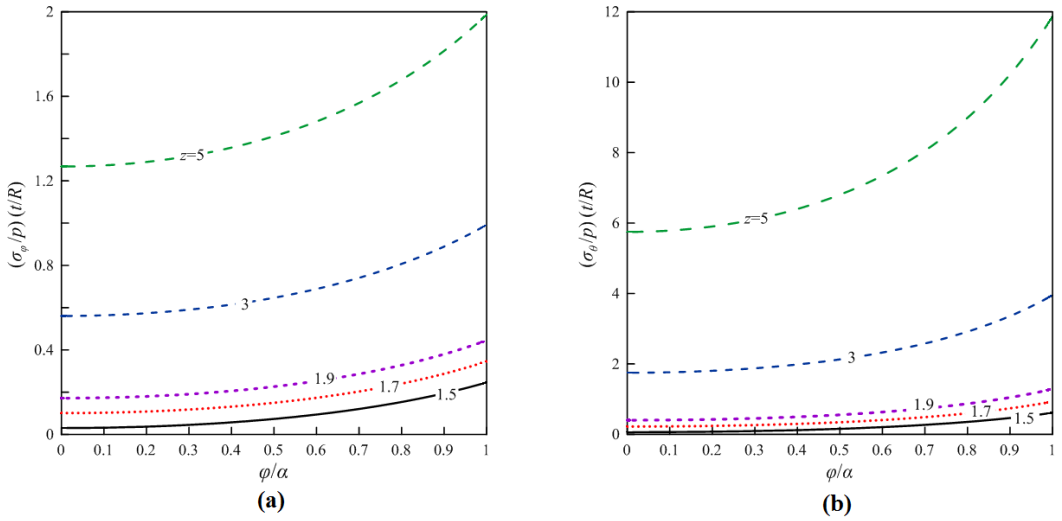

Fig. 23. Stress distribution for closed-end concave vessel with $\alpha = 45°$, a) Longitudinal stress (σ_φ), and b) Hoop stress (σ_θ).

When the lid is added to the vessel, for all the cases, the longitudinal stress increases, and simultaneously, a more uniform distribution of longitudinal stress is observed. The reason is somehow clear, because the zero longitudinal stress on the edge, for an open-end vessel, is replaced by a tensile longitudinal stress along the edge, for a closed-end vessel. However, the effect of adding the lid on the hoop stress is not the same for convex and concave vessels. In a convex vessel, due to the direction of the longitudinal stress which is applied by the lid, the opening of the vessel tends to shrink; hence, the hoop stress decreases. But, in a concave vessel, the direction of tensile longitudinal stress on the edge makes the opening to expand, and this results in increasing the hoop stress.

5. Conclusions

In this paper an analytical study of stress distribution in a special type of thin-walled pressure vessel was presented. The vessel is a surface of revolution generated by rotating a circular arc about an axis that neither intersects the arc nor necessarily passes through the arc center. Two types of convex and concave vessels with both of open- and closed-end conditions were investigated. As a result of this study, closed-form equations were derived for the stress components within the vessel wall, caused by the internal pressure. Since this type of vessel was not studied in the previous researches, the present analytical results were compared with those of Finite Element (FE) simulations. The results are summarized as follows:

1. A very close agreement between analytical results and Finite Element (FE) simulations was observed, which evidently shows the validity of the analytical model.

2. Using the proposed analytical model, the effect of different geometric parameters on the stress distribution was studied. The results show that the stress state in a closed-end convex vessel, in which the symmetry axis passes through the center of the generative arc, is the same as that of a thin-walled spherical pressure vessel.

3. When the lid is added to the vessel, the longitudinal stress increases and simultaneously becomes more uniformly distributed.

4. The effect of lid in the hoop stress in convex vessel and concave vessel are different. In convex vessel the hoop stress decreases if the lid is added to the vessel. Whereas in a closed-end concave vessel the hoop stress increases due to existence of the lid, when compared with similar open-end concave vessel.

References

[1] GH. Majzoobi, Strength of Materials, Bu-Ali Sina Univercity Press, (2006) (In persian).

[2] H.W. Bargmann, Prediction of pressure vessel failure: A critical review of the probabilistic approach, Theor. Appl. Fract. Mec., 5(1) (1986) 1-16.

[3] Y.M. Hwang, Y.K. Lin, Analysis and finite element simulation of the tube bulge hydroforming process, J. Mater. Process. Tech., 125-126 (2002) 821-825.

[4] M. Strano, T. Altan, An inverse energy approach to determine the flow stress of tubular materials for hydroforming application, J. Mater. Process. Tech., 146(1) (2004) 92-96.

[5] G.H. Rahimi, S.J. Roozegar, Elastic-Plastic analysis of a cylindrical pressure vessel with lids of variable thickness, In 13th Annual Conference of Mechanical Engineering, Isfahan University of Technology, Isfahan, Iran, (2005) (In Persian).

[6] K. Abrinia, M. Dehghani, A novel analysis of thick-walled pressure vessels under sudden internal pressure, considering the effects of strain hardening and strain rate, In 13th Annual Conference of Mechanical Engineering, Isfahan University of Technology, Isfahan, Iran, (2005) (In Persain).

[7] S. Boumaiza, J.P. Cordebois, M. Brunet, G. Nefussi, Analytical and numerical study on plastic instabilities for axisymmetric tube bulging, Int. J. Mech. Sci., 48(6) (2006) 674-682.

[8] S.R.X. Lopes, P.B. Goncalves, D.C. Pamplona, Influence of initial geometric imperfections on the stability of thick cylindrical shells under internal pressure, Commun. Numer. Meth. Eng., 23 (2006) 577-597.

[9] F. Djavanroodi, M. Gheisary, H. Zoghi-shal, Analytical and numerical analysis of free Bulge tube hydroforming, Am. J. Appl. Sci., 5(8) (2008) 972-979.

[10] R. Velasco, N. Boudeau, Tube bulging test: Theoretical analysis and numerical validation, J. Mater. Process. Tech., 205(1-3) (2008) 51-59.

[11] P. Bertot, E. Ceretti, C. Giardini, The determination of flow stress of tubular material for hydroforming applications, J. Mater. Process. Tech., 203 (2008) 381-388.

[12] A.H. Ben Ouirane , R. Velasco, G. Michel, N. Boudeau, Error evaluation on experimental stress–strain curve obtained from tube bulging test, Int. J. Mater. Form., 3(S1) (2010) 195-198.

[13] N. Boudeau, P. Male´cot, A simplified analytical model for post processing experimental results from tube bulging test: Theory, experimentation, simulations, Int. J. Mech. Sci., 65(1) (2012) 1-11.

[14] J. Kru˙zelecki, R. Proszowski, Shape optimization of thin-walled pressure vessel end closures, Struct. Multidisc. Optim., 46 (2012) 739-754.

[15] A. Chaaba, Reliability assessment by analytical calculation of the plastic collapse load of thin pressure vessels with strain hardening and large deformation, Thin Wall Struct., 62 (2013) 46-52.

[16] Z. He, S. Yuan, Y. Lin, X. Wang, W. Hu, Analytical model for tube hydro-bulging test, partI: Models for stress components and bulging zone profile, Int. J. Mech. Sci., 87 (2014) 297-306.

[17] Z. He, S. Yuan, Y. Lin, X. Wang, W. Hu, Analytical model for tube hydro-bulging tests, partII: Linear model for pole thickness and its application, Int. J. Mech. Sci., 87 (2014) 307-315.

[18] M. Zamani Nejad, P. Fatehi, Exact elasto-plastic analysis of rotating thick-walled cylindrical pressure vessels made of functionally graded materials, Int. J. Eng. Sci., 86 (2015) 26-43.

[19] M.E. Babeshko, A.Z. Galishin, A.I. Semenets, Yu.N. Shevchenko, Influence of the stress mode on the strength of high-pressure vessels, Int. Appl. Mech., 51(3) (2015) 319-325.

[20] A. Ibrahim, Y. Ryu, M. Saidpour, Stress analysis of thin-walled pressure vessels, Mod. Mech. Eng., 5(1) (2015) 1-9.

[21] J. Mulder, H. Vegter, H. Aretz, S. Keller, A.H. van den Boogaard, Accurate determination of flow curves using the bulge test with optical measuring systems, J. Mater. Process. Tech., 226 (2015) 169-187.

[22] X.L. Cui, X.S. Wang, S.J. Yuan, The bulging behavior of thick-walled 6063 aluminum alloy tubes under double-sided pressures, JOM, 67(5) (2015) 909-915.

[23] B. Liu, W. Wu, Y. Zeng, Pressure-time loading profile for tube superplastic free bulging, Int. J. Adv. Manuf. Tech., 92(5-8) (2017) 2267-2278.

[24] X.L. Cui, Z.P. Yang, X.S. Wang, Characterization of multiaxial stress-strain response of tube metal from double-sided hydro-bulging test based on Hosford's 1979 yield criterion, JOM, 69(5) (2017) 930-936.

[25] K. Wu, X. Li, Y. Ge, S. Ruan, Determination of tubular material parameters in bulging test with three-dimensional digital image correlation method, Int. J. Adv. Manuf. Tech., 96(5-8) (2018) 2091-2099.

[26] X. Song, H. Hui, Tube material properties determination and final forming pressure calculation of hydraulic formed corrugated tubes, J. Press. Vessel Technol., 141(6) (2019) 061408.

[27] ASM Handbook, Properties and Selection: Irons, Steels, and High-Performance Alloys, Volume 1, ASM International, (1990).